Effect of surface conditioning on zinc nucleation using aluminium cathodes

T. XUE, W. C. COOPER, R. PASCUAL, S. SAIMOTO

Department of Metallurgical Engineering, Queen's University, Kingston, Ontario K7L 3N6, Canada

The effect of the aluminium cathode microstructure on zinc nucleation has been investigated through surface examination by SEM and cyclic voltammetry. Zinc nucleation is strongly affected by the surface preparation and impurities present in the aluminium. For chemically pure aluminium, the oxide film on the surface plays an important role during zinc nucleation and crystal growth. Thickening the barrier oxide film inhibits nucleation while a reverse effect can be obtained by thinning or removing the oxide film. In the case of a dilute aluminium with iron alloy, following anodization, the Al–Fe intermetallic phases provide conductive paths through the oxide film resulting in zinc nucleation.

1. Introduction

The nucleation of metal electrodeposits onto different substrates during electrolytic processes is an important phenomenon in defining the nature of the deposits and their strippability [1, 2]. What is noticeably lacking are definitive studies on the nucleation process in relation to the substrate and the stripping process. Such knowledge is important in the electrolytic production of metal powders and of metal deposits which are to be subjected to automated stripping.

Many studies of the extraction of zinc from electrolytic solutions through electrodeposition on aluminium cathodes have been carried out in the field of zinc electrowinning [3-29]. However, due to the complex nature of the industrial operation, our understanding of the zinc electrowinning process is still limited.

According to its standard potential, zinc (-0.763 V) is less noble than hydrogen and most transition metals such as copper, nickel, and iron. Although most of the impurities have been removed from the electrolyte during the purification process, small amounts are inevitably present in the solution. Those impurities which are more noble than zinc will be codeposited during the electrolysis. According to previous work, the presence of small or even trace amounts of certain metallic impurities in the zinc electrolyte may greatly affect the current efficiency and the deposited zinc morphology. For example, when the germanium content in the solution increases to about 1 p.p.m., the current efficiency decreases from above 90% to less than 20% [16]. Therefore, it is not suprising that most of the previous work has concentrated on aspects of solution composition. For the past two decades, a systematic investigation of the related metallic impurities contained in zinc electrolyte has been carried out by Mackinnon *et al.* [3, 11, 16, 23, 25].

According to this literature, the decrease in current efficiency is mainly attributable to the low hydrogen overpotential of the codeposited impurities [3]. However, the reasons for the change in the crystal orientation of the deposited zinc in the presence of the metallic impurities are still not clear.

So far little attention has been paid to the effects of the aluminium cathode on zinc electrowinning, including impurities in the aluminium, surface orientation, surface pretreatment as well as corrosion behaviour. In fact, the surface state of the aluminium cathode may play an important role in the zinc nucleation process. It is known that a compact aluminium oxide film is always present on the aluminium surface. This oxide film determines the conduction, corrosion and nucleation behaviour taking place on the aluminium surface [30]. The surface oxide film and its properties, on the other hand, are closely related to the impurities contained in the aluminium and the surface treatment procedure. Previously, Mackinnon and Brannen [5] reported that for commercially pure aluminium, the fine-grained cathodes had more zinc nucleation sites than large-grained cathodes and zinc nucleation was easier on the etched aluminium cathode than on the unetched one. Moreover, in practice, it has been observed for a long time that sometimes the deposited zinc is firmly bound to the surface of the aluminium substrate so that the removal or stripping of the zinc is difficult or even impossible. This phenomenon is called 'sticking'. It has been reported that the presence of corrosive anions such as fluoride ions in the zinc electrolyte is the main reason for 'sticking' [30-37]. Although the influence of electrolyte impurities on the adhesive strength of zinc electrodeposited on aluminium has been studied [35], the relationship between the corroded aluminium cathode and high zinc adhesion has not been systematically investigated.

In order to elucidate further the fundamental par-

ameters and/or conditions which determine the zinc nucleation on an aluminium substrate, the present work has concentrated on the microstructural aspects of the aluminium cathode and on the nucleation of the zinc particles. The effects of the oxide film, impurities in the aluminium as well as different surface pretreatment of the cathode on the zinc nucleation have been considered.

2. Experimental details

2.1. Materials

Analytical grade $ZnSO_4 \cdot 7H_2O$ (0.0005% Cl, no detectable F), H_2SO_4 (0.0002% Cl, no detectable F) and NaF from BDH and deionized distilled water were used in this work. Superpure aluminium (99.999%) and aluminium-iron alloy (0.715% Fe, 0.005% Mg, 0.004% Cu, 0.006% Mn, 0.040% Si, 0.006% Cr and 0.004% Zn) sheets supplied by Alcan International Ltd were used as cathodes. The pure aluminium samples were annealed at $310°C$ for 1 h while the Al–Fe alloy samples were annealed at $400°C$ for 2 h. Although the grain sizes determined by electron channelling contrast did not appear ideally equiaxed, the averaged diameters were 25 and $30 \mu m$ respectively using the intercept method. The cathode was covered by acrylic resin except the working face with diameter of 1 cm. The connection was made with a copper wire through a hole at the back of the holder.

2.2. Surface treatment

The aluminium cathodes were abraded with emery paper from 200 to 600 mesh, electropolished in 1 : 4 perchloric acid/ethanol solution surrounded with dry CO_2 at 20 V for ~3–4 min, and rinsed with distilled water. To increase the thickness of the surface oxide film, anodizing was carried out in 15 wt % H_2SO_4 solution under a current density of $25 mA cm^{-2}$ for 5 min.

2.3. Electrodeposition and surface examination

The electrochemical measurements of the zinc electrolyte were conducted in a three-electrode single compartment cell. A platinum or a graphite electrode was used as the counter electrode and the reference electrode was a Ag/AgCl microelectrode (Microelectrode, Inc.) and was purged with pure N_2 prior to measurement. The zinc electrolyte consisted of 1 M H_2SO_4 and 0.3 M $ZnSO_4$. An EG&G Princeton Model 170 electrochemical system was used for the polarization measurements and as a power source. To eliminate the possibility of chloride contaimination effect on the zinc nucleation, the runs for surface examinations were performed without the reference electrode in a clean solution purged with pure nitrogen. The current density used was $25 mA cm^{-2}$ and the process was carried out at room temperature. After zinc was deposited on the aluminium cathode for the desired time,

the sample was taken out quickly from the solution, carefully rinsed with distilled water and ethanol, and dried.

The SEM and EDS examinations were carried out using a JEOL JSM 840 scanning electron microscope. A layer of carbon film was deposited on the sample surface to prevent charging of the non-conducting Al_2O_3 film.

3. Results and discussion

3.1. SEM examination

3.1.1. Pure aluminium cathode. The SEM photomicrographs of the zinc deposits on the electropolished pure aluminium cathodes are shown in Fig. 1. During these deposition times, a few hydrogen bubbles were observed. From Fig. 1a it can be seen that in 1 min, a few zinc nuclei appear on the aluminium surface. Since the surface of the cathode is relatively smooth, the initial nucleation starts at isolated spots. The zinc clusters are polygonal in shape and are composed of small hexagonal platelets randomly oriented to one another. Subsequent deposition either occurs on the initial zinc nuclei by joining one edge site to another or by forming new nuclei (see Fig. 1b).

For pure aluminium, it is well known that upon exposure to air or in aqueous solutions, a compact amorphous oxide film (Al_2O_3) with a thickness in the range of 1 to 5 nm is quickly formed [38–40]. As a
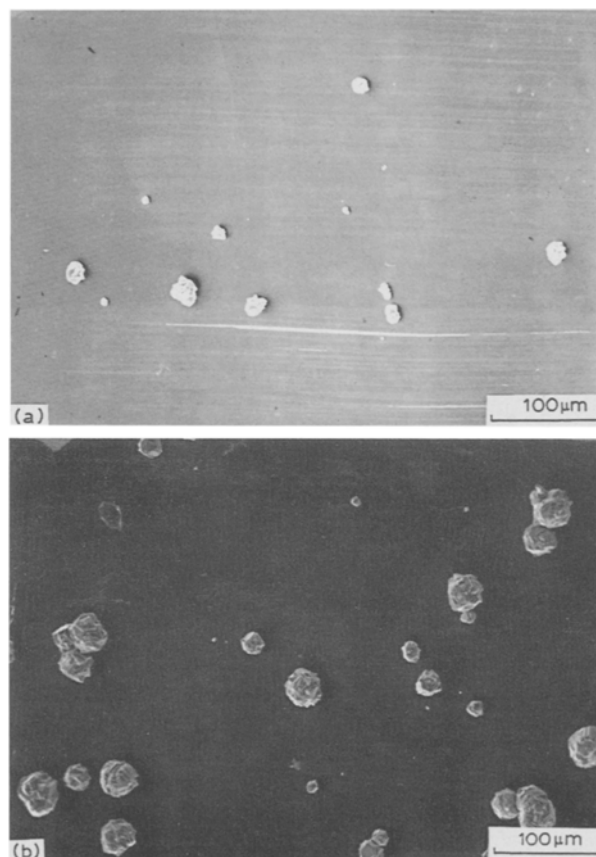

Fig. 1. SEM micrographs on zinc nucleation and pure aluminium cathode as a function of time. Solution: 1 M H_2SO_4 + 0.3 M $ZnSO_4$; current density $25 mA cm^{-2}$; (a) 1 min, (b) 5 min. Magnification: 200×.

result, the controlling interface during zinc electro-deposition is that of Al_2O_3 with the solution. Kerby [29] pointed out that it is just the presence of this aluminium oxide film which prevents the high adhesion of the deposited zinc on the surface. On the other hand, aluminium oxide is also known to be an electrical insulator. However, whenever an external potential is applied, a relatively high electric field (it can be as high as $10^7 \, V cm^{-1}$) is set up across such a thin oxide film so that a 'high-field ionic conduction' is realized [38].

It is clear that for the pure aluminium substrate, even under the present relatively high current density, the number of zinc nuclei is limited and the crystal growth is low. This means that the formation of a uniform oxide film on the pure aluminium surface results in a relatively high resistance across the oxide film so that the nucleation of zinc becomes difficult. Since the oxide film usually contains a large number of flaws which correspond to weak spots on the surface [40], it is reasonable to expect that the zinc deposition on the pure aluminium may start mainly around these lower resistance points. To pursue this reaction systematically it must be realized that the aluminium surface is influenced by a series of surface treatment procedures such as electropolishing and etching. During the anodizing process in sulphutic acid solution, a duplex film, i.e., a barrier layer (~ 10–20 nm) covered by a porous layer [38–40], can be formed. The thickness of the barrier layer depends on the applied potential ($\sim 1.4 \, nm \, V^{-1}$). Under the present conditions

($\sim 18 \, V$), the thickness of the barrier layer is estimated to be in the range of about 20 nm. Hence plating on the anodized surface would result in a reduced number of nuclei and make the observation of single sites possible. Figure 2 shows the results of zinc deposition on the anodized pure aluminium cathode at $25 \, mA \, cm^{-2}$ for 1 min. As expected, the number of zinc nuclei is much less than in the case of the sample without the anodizing treatment (comparing with Fig. 1a). The hydrogen evolution under these conditions was also not noticeable. The morphology of the nuclei (see Fig. 2b) is hexagonal with platelets parallel to (0 0 2), and attached perpendicular to the electrode surface. Therefore, the anodizing on the pure aluminium cathode greatly affects the zinc nucleation and crystal growth. Moreover, this observation clearly shows that the rapid growth direction of the zinc nuclei lies on the basal plane.

According to the above description, the thickening of the oxide film on the pure aluminium cathode makes the zinc deposition more difficult. In contrast, if the oxide film can be thinned or removed, more zinc nucleation sites and a higher crystal growth rate can be expected. It is known that fluoride ions can rapidly remove the oxide film on an aluminium surface by uniform dissolution [41–46]. In this work, when an electropolished pure aluminium cathode was immersed into a zinc electrolyte containing 0.1 M NaF for 10 min before the zinc deposition was started, a totally different pattern of zinc nucleation was observed after 1 min deposition as shown in Fig. 3. The zinc nucleation sites are dramatically increased. A detailed description of the corrosion of the aluminium cathode as well as the zinc nucleation in the presence of F^- will be presented in a later publication. The results shown in Figs 1 to 3, however, confirm the importance of the aluminium oxide film during the zinc nucleation process.

3.1.2. Al–Fe alloy. The composition of the commercially used aluminium cathodes is: Fe 0.215, Si 0.130, Ti 0.005, Zn 0.003, Ga 0.013, Va 0.0065, Cu 0.006, in wt %. It is known that most of the metallic elements
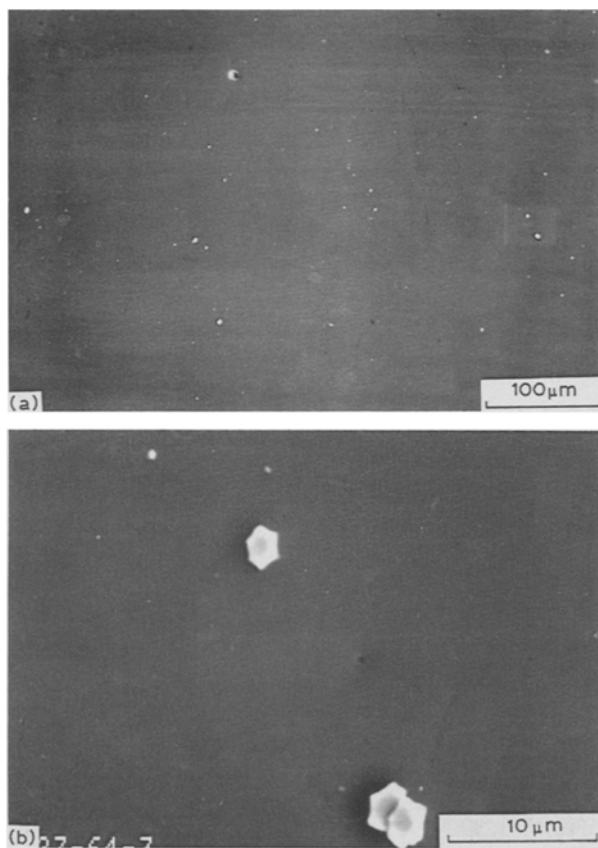

Fig. 2. SEM micrographs of zinc nucleation on anodized pure aluminium cathode for 1 min. Solution: 1 M H_2SO_4 + 0.3 M $ZnSO_4$; current density 25 mA cm^{-2}. Magnifications: (a) $200 \times$, (b) $2700 \times$.
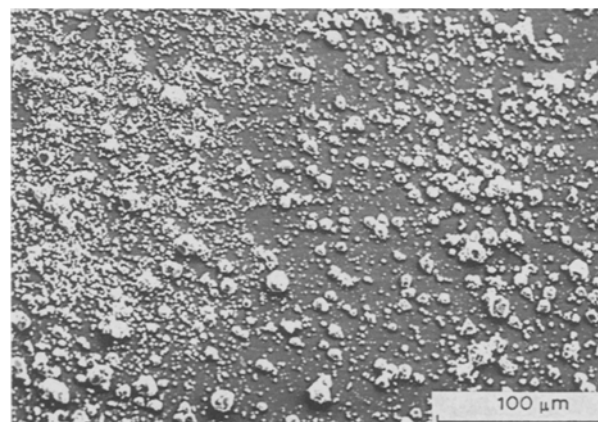

Fig. 3. SEM micrograph showing of the effect of fluoride ion on zinc deposition at 25 mA cm^{-2}. The pure aluminium cathode was immersed in 1 M H_2SO_4 + 0.3 M $ZnSO_4$ + 0.1 M NaF for 10 min before zinc deposition for 1 min. Magnification: $300 \times$.
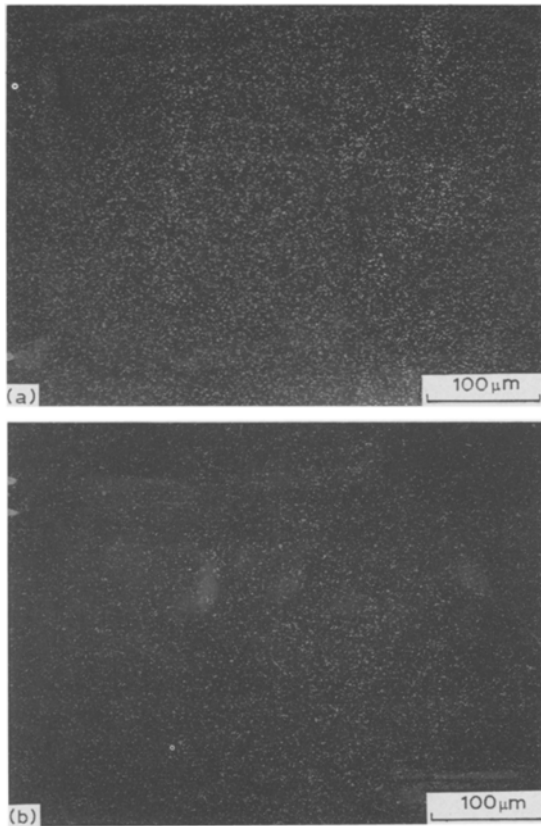
Fig. 4. X-ray mappings of iron in Al–Fe alloy samples. (a) Not anodized, (b) anodized. Magnification: 200 ×.

Fig. 5. SEM micrographs of zinc nucleation on unanodized Al–Fe cathodes as a function of time. Solution: 1 M H_2SO_4 + 0.3 M $ZnSO_4$; current density 25 mA cm^{-2}; (a) 1 min, (b) 5 min. Magnification: 200 ×.

readily alloy with the aluminium and the addition of alloying elements can improve the physical and mechanical properties of the aluminium [47–49]. In the present work, in order to eliminate the number of variables, only the behaviour of iron on zinc nucleation process was investigated.

The X-ray mappings of iron in the Al–Fe alloy samples are shown in Fig. 4. Based on Fig. 4a, bright points, which correspond to iron-rich particles, are uniformly distributed across the surface. A similar particle distribution can still be observed after the sample was anodized (see Fig. 4b). However, the particle density on the surface is lower compared with Fig. 4a.

Based on binary Al–Fe phase diagram, the common stable intermetallic phase is $FeAl_3$ [47]. However, a number of Al–Fe intermetallic phases such as $FeAl_6$, $FeAl_m$ have been observed in the commercial alloy, depending on the composition and cooling rates [50]. It should also be noted that the solubility of iron in aluminium is very low, about 2 p.p.m. at 400° C [47]. It is for this reason iron is used to control grain size with little effect on the aluminium matrix properties [51].

The SEM photomicrographs of zinc deposits on the electropolished Al–Fe alloy cathodes are shown in Fig. 5. Under the same experimental conditions as in the case of pure aluminium, a large number of zinc nuclei appear on the surface in 1 min (Fig. 5a). Although some nuclei have overlapped through crystal growth, many newly formed zinc nuclei (small
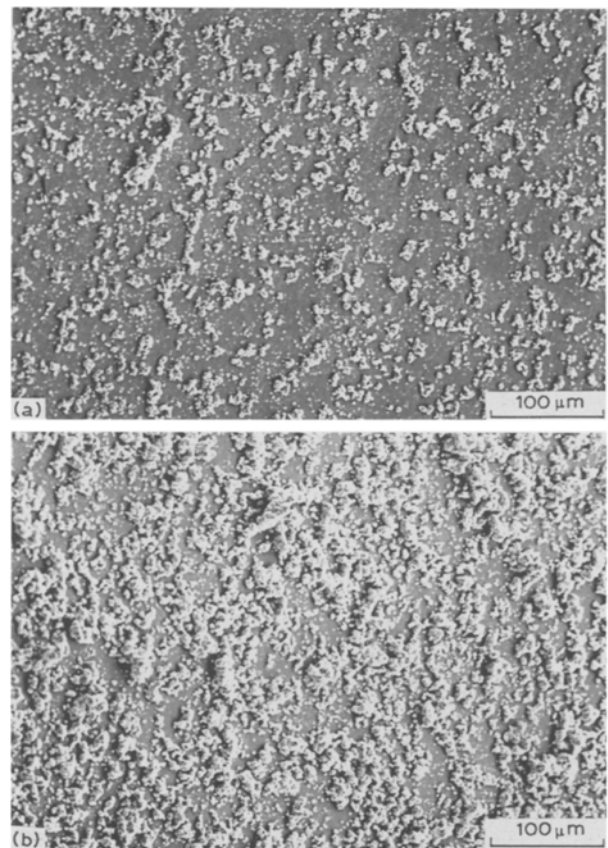
particles) can be clearly seen. This means that the available nucleation sites on the Al–Fe are much more numerous than in the case of pure aluminium. After 5 min, the initial nuclei have developed further and are overlapped while many new smaller nuclei can be identified as shown in Fig. 5b. Thus the presence of alloying elements can influence significantly the electrochemical behaviour of the aluminium.

Since the intermetallic phases such as iron and silicon compounds inhibit the formation of the aluminium oxide film on the surface of these particles, these intermetallic phases may act to accelerate the corrosion of aluminium in aqueous solutions [52]. According to previous work, iron is one of the major causes of the decrease in the corrosion resistance of aluminium so that the corrosion resistance of the aluminium containing iron can be improved markedly once the iron-rich particles are removed from the aluminium surface by cathodic polarization [53, 54]. On the other hand, these intermetallic phases may also behave as high electronic conductive spots within the surface oxide [55]. Therefore, in the case of zinc deposition, the presence of alloying metals may give rise to more available nucleation sites so that the nucleation process is greatly improved.

After the Al–Fe alloy was anodized in H_2SO_4 solution, a different zinc nucleation pattern was observed as shown in Fig. 6. It can be seen that the zinc nucleation and crystal growth were developed from isolated points and not many new nuclei can be
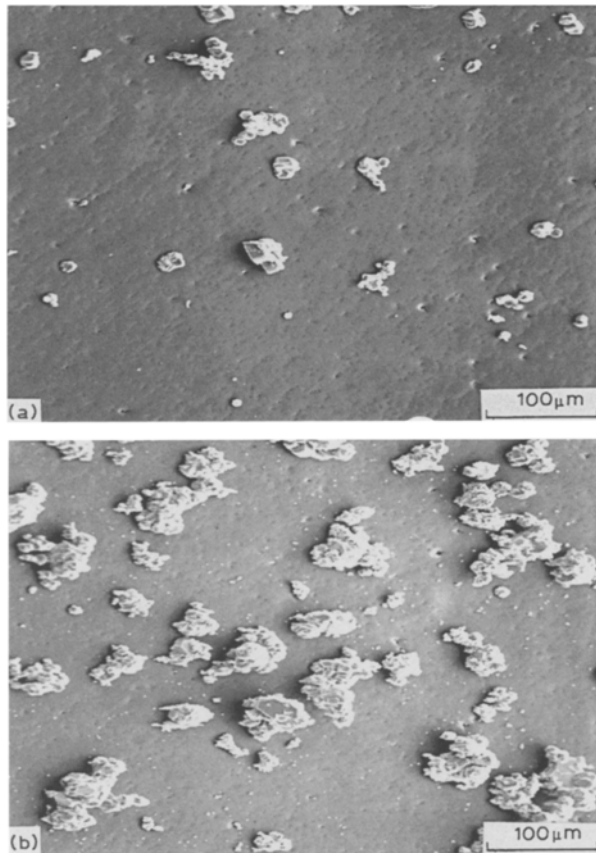
Fig. 6. SEM micrographs of zinc nucleation on anodized Al–Fe cathodes as a function of time. Solution: 1 M H_2SO_4 + 0.3 M $ZnSO_4$; current density 25 mA cm^{-2}; (a) 1 min, (b) 5 min. Magnification: 200 ×.

Fig. 7. Cyclic voltammograms for pure aluminium cathode in 1 M H_2SO_4 + 0.3 M $ZnSO_4$ solution. Scan rate 20 mV s^{-1}. (a) Not anodized, (b) anodized.

observed. According to Fig. 4, it is suggested that when the Al–Fe sample was anodized, the thickness of the oxide film on the surface increased thereby decreasing the number of iron-rich particles exposed to the solution, although the Al–Fe intermetallic phase is still present within the surface film. As in the case with pure aluminium, the anodizing does have a profound effect on the nucleation behaviour on the Al–Fe alloy. However, the presence of particles prevents a total sealing of the surface so that the nucleation can still be realized at a relatively high speed through the highly conductive iron-containing areas. The zinc nucleation and crystal growth at these isolated spots can be observed in Fig. 6a and 6b.

3.2. Cyclic voltammetry

In the present work, the effects of the aluminium cathode microstructure on zinc nucleation were investigated by cyclic voltammetry. The voltammograms obtained for zinc deposition on pure aluminium and Al–Fe alloy cathodes are shown in Figs 7 to 9.

For pure electropolished aluminium (Fig. 7a), the cycle starting from point A goes through a region of low current until at point C ($\sim$ 1.0 V/SHE) the current rapidly increases indicating the start of zinc deposition and hydrogen reduction. At point D, the sweep is reversed upon which the current continues to rise to a maximum point E and then decreases to point B where
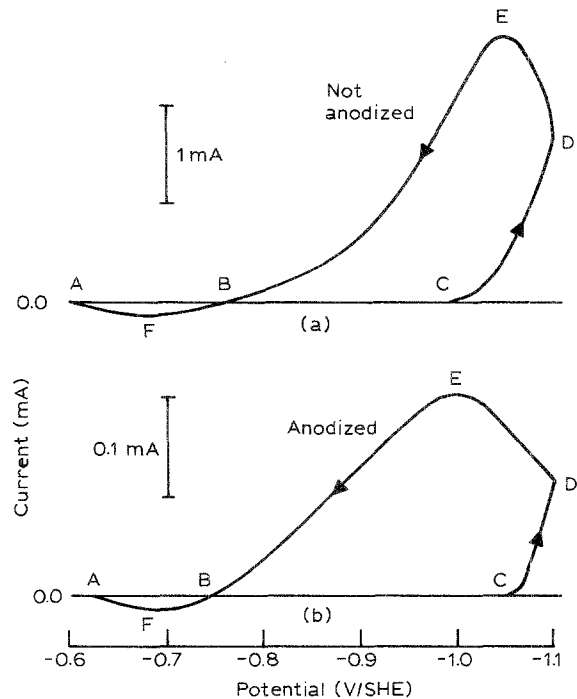
the anodic dissolution starts. The anodic peak is reached at point F and the stripping is completed on return to A.

When the aluminium was anodized, a similar behaviour was observed as shown in Fig. 7b. However, the potential at point C, the beginning of zinc deposition and/or hydrogen ion reduction, has been shifted to a more negative value ($\sim$ − 1.06 V). Moreover, in comparison with Fig. 7a, the corresponding current is much lower (just about 1/10 of the former).
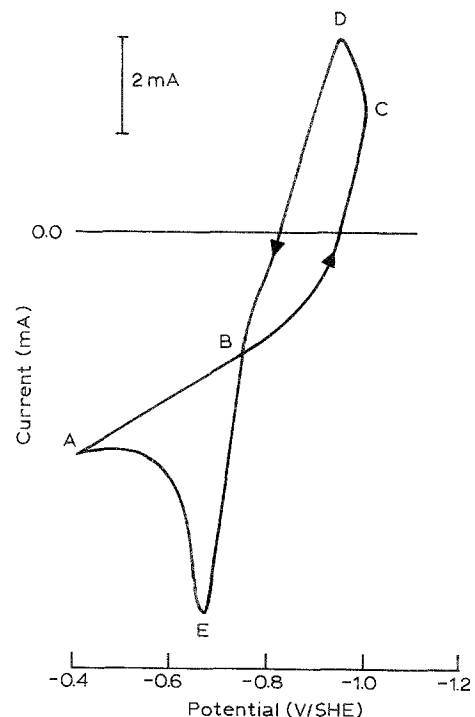

Fig. 8. Cyclic voltammogram showing effect of fluoride ion on zinc deposition on the pure Al cathode. Solution: 1 M H_2SO_4 + 0.3 M $ZnSO_4$ + 0.1 M NaF; scan rate: 20 mV s^{-1}.
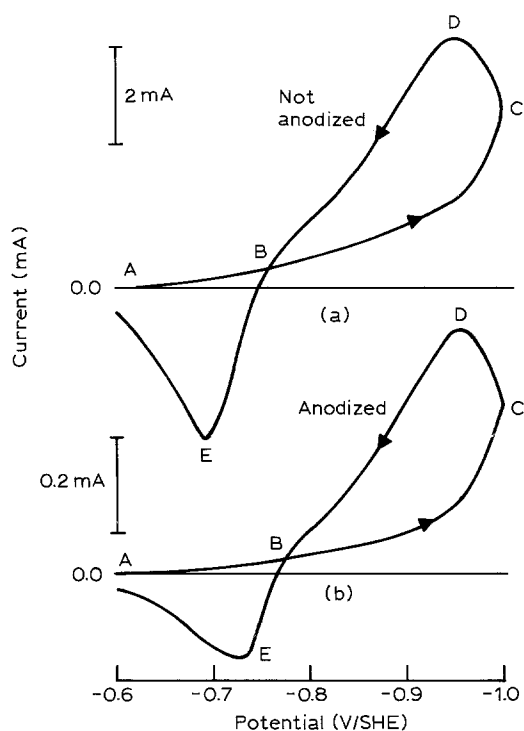
Fig. 9. Cyclic voltammograms for Al–Fe alloy cathode in 1 M H_2SO_4 + 0.3 M $ZnSO_4$ solution. Scan rate $20\,mVs^{-1}$. (a) Not anodized, (b) anodized.

The effect of fluoride ions in zinc deposition was also examined by cyclic voltammetry (Fig. 8). In the presence of F^-, the nucleation loop of the pure aluminium cathode has been significantly changed compared to Fig. 7a. A strong anodic dissolution of aluminium appears and higher cathodic current is observed.

The cyclic voltammograms for the Al–Fe alloy cathode are shown in Fig. 9. In the absence of anodizing (Fig. 9a), the current is relatively high and increases almost from the starting point A (~ -0.64 V). The cathodic and anodic maxima can be observed at points D and E respectively. After the Al–Fe cathode was anodized, similar cyclic voltammograms were observed (Fig. 9b) except that the current was much lower. In fact, the shape of the voltammograms observed in Fig. 9 is similar to that previously reported [28].

The cyclic voltammograms correlate with the results obtained from the SEM analysis. For pure aluminium, the high resistance of the oxide film gives rise to a more negative potential for zinc nucleation and hydrogen ion reduction. Based on Fig. 7a, the area covered by the cathodic curve (or nucleation loop) is much greater than that covered by the anodic curve. This indicates that the main reaction during the cathodic scanning is the reduction of hydrogen. When the thickness of the oxide film is increased by anodizing, conduction through the surface becomes more difficult so that the overpotential is further enhanced and the current decreases. A sharp increase in anodic area in Fig. 8 indicates a strong dissolution of aluminium in the zinc electrolyte containing F^- while the zinc deposition and hydrogen ion reduction start at more positive potentials. If the effect of aluminium dis-

solution can be discounted by considering only the area surrounded by curve ABE, the result strongly suggests that the main cathodic reaction is due to that of the zinc deposition. Furthermore Fig. 8, indicates that the effects of F^- on both aluminium corrosion and zinc deposition can be revealed by studying the related polarization. A detailed analysis of the effect of F^- will be described in a later paper.

For aluminium alloyed with iron, the Al–Fe intermetallic phase within the oxide film appears to provide active-sites for zinc deposition and hydrogen reduction. This suggests that the anodizing process does not deposite a barrier film on the Al–Fe particles. The low hydrogen potential of the iron-rich phase results in the start of the hydrogen reduction at a more positive potential. However the noticeably increased anodic area (compared to Fig. 7a) also suggests a decreased overpotential for zinc deposition since the applied potential at C is similar to that in Fig. 7a. Thus it can be concluded that the cathode with iron-rich particles has better electro-catalytic properties for zinc deposition. After the cathode was anodized, the thickness of the oxide film on aluminium matrix was increased but not on the iron-rich particles. As a result, similar cyclic voltammograms were obtained. However, since the available active sites for zinc nucleation are decreased through particle occlusion by the oxide layer, the cathodic current is also decreased.

4. Conclusions

The microstructure of an aluminium cathode plays an important role during the zinc deposition. The increase or decrease of the thickness of oxide film on the pure aluminium cathode will inhibit or enhance the zinc nucleation and crystal growth. The presence of alloying elements in aluminium affects the electrochemical behaviour of the cathode as regards the nucleation and crystal growth of zinc. The Al–Fe intermetallic phase greatly improves the zinc nucleation behaviour by providing highly conductive areas within the surface oxide film.

Acknowledgements

References

[1]   G. M. Rao and W. C. Cooper, *Hydrometall.* 4 (1979) 185–207.
[2]   K. S. Fraser and W. C. Cooper, *Surf. Tech.* 8 (1979) 385–98.
[3]   D. J. Mackinnon, J. M. Brannen and P. L. Fenn, *J. Appl. Electrochem.* 17 (1987) 1129–43.

[4]   T. Biegler and J. Frazer, *ibid.* **16** (1986) 654–62.
[5]   D. J. Mackinnon and J. M. Brannen, *ibid.* **16** (1986) 127–33.
[6]   A. Papachristodoulou, F. R. Foulkes and J. W. Smith, *ibid.* **15** (1985) 581–90.
[7]   T. N. Andersen, R. C. Kerby and T. J. O'Keefe, *J. Metals* **1** (1985) 36–43.
[8]   T. Biegler and D. A. Swift, *Hydrometall.* **6** (1981) 299–309.
[9]   E. J. Frazer and T. Lwin, *J. Appl. Electrochem.* **17** (1987) 453–62.
[10] T. J. O'Keefe, *Electroanal. Chem.* **168** (1984) 131–46.
[11] D. J. Mackinnon, J. M. Brannen and R. M. Morrison, *J. Appl. Electrochem.* **18** (1988) 252–56.
[12] D. J. Mackinnon, J. M. Brannen and P. L. Fenn, *ibid.* **16** (1986) 899–906.
[13] D. J. Mackinnon, *ibid.* **15** (1985) 953–60.
[14] D. J. Mackinnon, R. M. Morrison and J. M. Brannen, *ibid.* **16** (1986) 53–61.
[15] D. J. Mackinnon and P. L. Fenn, *ibid.* **14** (1984) 701–07.
[16] *Idem, ibid.* **14** (1984) 467–74.
[17] D. R. Fosnacht and T. J. O'Keefe, *Metall. Trans. B* **14B** (1983) 645–53.
[18] F. R. Foulkes, J. W. Smith, R. Kalia and D. W. Kirk, *J. Electrochem. Soc.* **128** (1981) 2307–14.
[19] Y.-M. Wang, T. J. O'Keefe and W. J. James, *ibid.* **127** (1980) 2589–93.
[20] D. R. Fosnacht and T. J. O'Keefe, *J. Appl. Electrochem.* **10** (1980) 495–504.
[21] R. Fratesi, G. Roventi, M. Maja and N. Penazzi, *ibid.* **10** (1980) 765–774.
[22] I. W. Wark, *ibid.* **9** (1979) 721–30.
[23] D. J. Mackinnon, J. M. Brannen and R. C. Kerby, *ibid.* **9** (1979) 71–9.
[24] *Idem, ibid.* **9** (1979) 55–70.
[25] D. J. Mackinnon and J. M. Brannen, *ibid.* **7** (1977) 451–39.
[26] R. C. Kerby, H. E. Jackson and T. J. O'Keefe, *Metall. Trans. B* **8B** (1977) 661–68.
[27] B. A. Lamping and T. J. O'Keefe, *Metall. Trans. B* **7B** (1976) 551–58.
[28] T. Biegler, in 'Application of Polarization Measurements in the Control of Metal Deposition' (edited by I. H. Warren), Elsevier, New York (1984) pp. 32–46.
[29] R. C. Kerby, in *ibid*, pp. 84–132.
[30] J. Gruberger and E. Gileadi, *Electrochim. Acta* **31** (1986) 1531–40.
[31] F. H. C. Kelly, *J. Electrochem. Soc.* **101** (1954) 239–43.
[32] A. I. Levin, A. V. Pomosov and T. A. Tkachenko, *J. Appl. Chem. USSR* **26** (1953) 1189–93.

[33] R. Kammel and M. H. Saadat, *Metall.* **30** (1976) 551–55.
[34] P. Andrianne, J. Scoyer and R. Winand, *Hydrometall.* **6** (1980) 159–69.
[35] M. Goektepe, M. Guelbas and R. Kammel, *Erzmetall.* **37** (1984) 289–94.
[36] R. Kammel, M. Goektepe and H. Oelmann, *Hydrometall.* **19** (1987) 11–24.
[37] E. R. Cole, Jr., L. L. Smith and M. M. Fine, US Bureau of Mines, 8344 (1979).
[38] S. Tajima, in 'Advances in Corrosion Science and Technology' (edited by M. G. Fontana and R. W. Staehle), vol. 1, Plenum Press, New York (1970) pp. 229–362.
[39] P. Csokan, in *ibid.*, vol. 7, Plenum Press, New York (1980) pp. 239–356.
[40] G. E. Thompson and G. C. Wood, in 'Treatise on Materials Science and Technology' (edited by J. C. Scully), vol. 23, Academic Press, New York (1983) pp. 205–330.
[41] K. F. Lorking and J. E. O. Mayne, *Brit. Corros.* **1** (1966) 181–82.
[42] J. A. Richardson and G. C. Wood, *J. Electrochem. Soc.* **120** (1973) 193–202.
[43] M. Katch, *Corros. Sci.* **8** (1968) 423–31.
[44] J. Radosevic, Z. Mentus, A. Djordjevic and A. R. Despic, *J. Electroanal. Chem.* **193** (1985) 241–54.
[45] R. J. Tzou and H. C. Shih, *Corros. Sci.* **45** (1989) 328–33.
[46] K. Haffe, in 'DECHEMA Corrosion Handbook' (edited by D. Behrens), vol. 1, VCH Publishers, New York (1987) pp. 109–13.
[47] L. F. Mondolfo, 'Aluminium Alloys: Structure and Properties', Butterworths, London (1976).
[48] D. Altenpohl, 'Aluminium Viewed from Within', Aluminium-Verlag, Düsseldorf (1982).
[49] J. E. Hatch, Aluminium, Properties and Physical Metallurgy, ASM (1984).
[50] P. Liu and G. L. Dunlop, *Acta Metall.* **6** (1988) 1481–89.
[51] S. Saimoto, H. Sang and L. R. Morris, *Acta Metall.* **29** (1981) 215–28.
[52] K. Nisancioglu and O. Lunder, in 'Aluminium Alloys. their Physical and Mechanical Properties' (edited by E. A. Starke, Jr. and T. H. Sanders, Jr.), EMAS, West Midlands, UK (1986) pp. 1125–41.
[53] K. Nisancioglu, K. Y. Davanger and O. Strandmyr, *J. Electrochem. Soc.* **128** (1981) 1523–26.
[54] K. Nisancioglu, O. Lunder and H. Holtan, *Corros.* **41** (1985) 247–57.
[55] K. Wefers, *Aluminium* **57** (1981) 722–26.